Monitoring ice capped active Volcán Villarrica in Southern Chile by means of terrestrial photography combined with automatic weather stations and GPS

Andrés Rivera[1,2], Javier G. Corripio[3], Ben Brock[4], Jorge Clavero[5] and Jens Wendt[1]

[1] *Centro de Estudios Científicos, Avenida Arturo Prat 514, Valdivia, Chile*
E-mail:arivera@cecs.cl [2] *Universidad de Chile, Marcoleta 250, Santiago, Chile*
[3] *University of Innsbruck, Innsbruck, Austria*
[4] *University of Dundee, Scotland, UK*
[5] *Servicio Nacional de Geología y Minería, Avenida Santa María 0104, Santiago, Chile*

ABSTRACT. Volcán Villarrica (39°25′12″S, 71°56′27″W; 2847 m a.s.l.) is an active ice-capped volcano located in the Chilean Lake District. Monitoring of the surface energy balance and glacier frontal variations, using automatic weather stations and satellite imagery, has been ongoing for several years. In recent field campaigns, surface topography was measured using Javad GPS receivers. Daily changes in snow, ice and tephra-covered area were recorded using an automatic digital camera installed on a rock outcrop. In spite of frequently damaging weather conditions, two series of consecutive images were obtained in 2006 and 2007. These photographs were georeferenced to a resampled 90 m pixel size SRTM digital elevation model and the reflectance values normalised according to several geometric and atmospheric parameters. The resulting daily maps of surface albedo are used as input to a distributed glacier melt model during a 12 day midsummer period. The spatial pattern of cumulative melt is complex and controlled by the distribution of airfall and windblow tephra, with extremely high melt rates occurring downwind of the crater and exposed ash banks. Furthermore, the camera images are also used to visualise the pattern of glacier crevassing. The results demonstrate the value of terrestrial photography to understanding the energy and mass balance of the glacier, including the generation of melt water, and the potential value of the technique in monitoring volcanic activity and potential hazards associated with ice-volcano interactions during eruptive activity.

INTRODUCTION

Volcán Villarrica (Figure 1, 39°25′12″S, 71°56′27″W; 2847 m a.s.l.) is considered a highly active ice-capped volcano, which is characterized in historical times mainly by mild strombolian activity (González-Ferrán, 1995; Lara, 2004), permanent degassing and periodic explosions, with the lava lake remaining at a high level (90-180 m below surface) at least since 1984 and very sensitive to the magmatic conduit activity (Calder and others, 2004; Witter and Delmelle, 2004). Concentrations of acid gases measured at the summit of the crater have been recognized as a hazard to climbers ascending the volcano, who may be exposed to concentrations above limits defined by the U.S. National Institute of Occupational Safety and Health (Witter and Delmelle, 2004). Its historical eruptive activity (Petit-Breuihl and Lobato, 1994; Lara, 2004) indicates a low frequency of large explosive eruptions (Volcanic Explosivity Index, VEI between 3 and 4). More than 50 eruptive events, however, have been documented since 1558 (Petit-Breuihl and Lobato, 1994). The latest most violent eruption took place in 1971-72 when lava flows were generated, as well as 30 to 40 km h^{-1} laharic flows (Naranjo and Moreno, 2004) descending towards Lagos Villarrica and Calafquén (Figure 1). Lahars produced by eruptions of Volcán Villarrica in 1948-1949, 1963-1964, and 1971-1972 have resulted in the deaths of more than 75 people (Stern, 2004), and are considered the main hazard of the volcano (Moreno, 2000). The volcano is covered by a glacier of 30.3 km^2 (Rivera and others, 2006), mainly distributed towards the south and east where the main glacier basin (Glaciar Pichillancahue-Turbio, 17.3 km^2, Figure 2), composed of partially ash/debris-covered ice is located, partially infilling a volcanic caldera depression (Clavero and Moreno, 2004). The energy balance of this glacier has been monitored since 2003 (Brock and others, 2007), and Global Positioning System (GPS) as well as Radio Echo Sounding (RES) measurements were carried out in January 2005 (Rivera and others, 2006).

One of the most interesting direct effects of volcanic activity on the overlying glaciers is the ice cracking or crevassing observed before or during eruptive events (Klohn, 1963; Fuenzalida, 1976; González-Ferrán, 1995; Fuentealba and others, 1985). Ice cracking has been detected by seismicity (Metaxian and others, 2003), however here we propose to observe possible ice cracking by obtaining daily photographs of the ice. This process could be important for ice flow and for the hydrological balance of the glacier, as crevasses are the main pathway for meltwater to enter the glacier's en- and subglacial drainage system (Fountain and others, 2005; Fountain and Walder, 1998).

A second direct effect of volcanic activity is the deposition of pyroclastic materials on top of the glaciers, changing the albedo and affecting the energy balance by providing insulation from atmospheric heat and insolation where particles are large or the cover is continuous (Adhikary and others, 2002; Kirkbride and Dugmore, 2003). Studies of tephra thermal properties and glacier melt rates at Volcán Villarrica (Brock and others, 2007), identified a very low thermal conductivity of 0.35 W m^{-1} K^{-1} in the lapilli tephra which blankets most of the ablation zone. Furthermore, a critical thickness of just 5 mm of tephra cover was found to reduce the melt rate of the buried ice compared with a bare surface. Consequently, volcanically produced materials appear to have a large positive impact on the mass balance of glaciers on Volcán Villarrica, due to an extensive mantle of insulating tephra in the lower ablation zones. In this study quantitative assessment of the total area of tephra cover and tephra-free ice slopes and snow albedo have been made through terrestrial photography.

AIMS AND METHODS

The main aim of this paper is to analyse albedo variation and its impact on melt on Glaciar Pichillancahue-Turbio of Volcán Villarrica by means of terrestrial photography. Previous measurements of the glacier areal variations (Rivera and others, 2006) have been updated until year 2007 which permitted the assessment of recent ice retreat on the volcano's glaciers.

Meteorological data

The meteorological data were obtained by an automatic weather station (AWS) that was located during the summer on the surface of the glacier at 1933 m asl, near the Equilibrium Line Altitude, located at ∼2000 m a.s.l. during the year 2003/4 (Rivera and others, 2006). During the winter the AWS was moved to a location on a rock outcrop at 1925 m a.s.l., next to the fixed camera (Figures 2 and 3). The AWS recorded incoming and reflected shortwave radiation, net all-wave radiation, air temperature, air humidity and wind speed at 2 m above the surface with hourly mean values recorded on a Campbell CR10 data logger. Albedo was measured using a Kipp and Zonen CM6B albedometer sensitive to radiation in the range 0.3 - 2.8 μm, with the sensors mounted in a surface parallel plane. Details of the collected variables and technical details of the utilized sensors at the AWS are described in Brock and others (2007).

Oblique photography

For measuring albedo, surface changes and tephra cover, an automatic camera (Canon EOS 300D) was installed at the upper part of the rim surrounding the main volcano edifice (upper part of the caldera, Figure 2) from where daily photographs of the glacier were obtained. The camera has a 6.3 Megapixel CMOS sensor and recorded the images in a 2 GB flash card memory. It was fitted with a high quality, fixed 24 mm focal length lens to minimise optical distortions. This camera sensor has some sensitivity in the near infrared spectrum, at least to 1000 nm, and beyond that point if the IR filter is removed (experimental tests by the authors). The camera was inserted into a Pelikan sealed box where it was controlled by a Canon timer. The system was powered by 12-V batteries which were fed by a solar panel installed nearby.

Conventional photography is a powerful medium for collecting and storing information. If this information can be located precisely in space, then photography becomes a powerful tool for quantitative analysis. Here we use a tool for georeferencing oblique photography developed by Corripio (2004), using a single image and a digital elevation model (DEM). The accuracy of the technique will depend on the accuracy of the DEM and on the quality of the photographic image, especially the degree of distortion and aberration produced by the lens. This technique does not produce elevation data. It actually requires an existing DEM. What the tool does is to locate the geographical position of every pixel in a photographic image. It is therefore useful to map land cover and to assess surface cover change. This technique follows standard procedures for perspective views in computer graphics or photogrammetry (Fiume, 1989; Foley and others, 1990; Slama and others, 1980). Basically it consists in creating a virtual photography of the DEM that can then be scaled to the resolution of the photographic image to establish a mapping function between pixels in the photograph and grid cell points. This allows locating the exact position of pixels in the oblique image. The georeferencing process consists of a viewing transformation applied to the DEM in which the coordinates of every grid cell are firstly translated to refer them to a coordinate system with origin at the camera position. Then a transformation is applied according to the viewing direction and focal length of the camera. This results in a three dimensional set of points corresponding to the cells in the DEM as seen from the point of view of the camera. Finally, the resulting viewing transformation is projected into a two-dimensional viewing 'window', corresponding to the area of the film and scaled proportionally. The process is explained in detail by Corripio (2004), it has been coded in IDL under the Creative Commons license and it is freely available from the authors.

Using this technique the evolution of the snow cover was mapped accurately during the acquisition periods. Once the photograph is georeferenced, the reflectance values are normalized according to the viewing geometry, the angle of incidence of sun's rays on the slope, the ratio of direct to diffuse radiation, the atmospheric transmittance between the pixel location and the position of the camera, and the effect of radiation reflected from the surrounding slopes. The final result is a map of normalized reflectance values, or relative albedo. The atmospheric transmittance was calculated using the radiative transfer model MODTRAN (Berk and others, 1989) and general knowledge of the local atmospheric conditions from the AWS. The photographic image was mapped to a resampled DEM from the Shuttle Radar Topography Mission (SRTM, acquired by JPL/NASA in 2000). It is important to notice that the resampling procedure to a 10m resolution DEM cannot increase the actual resolution of the original DEM, at 90m, but allows the extraction of more information from the photography within the known spacial limits of the original DEM grid cell. The DEM was not contemporary to the photographic image acquisition. This may add some errors to the results, as the slope and aspect may be slightly different from one date to another, and the snow accumulation may change. It is completely out of our financial possibilities to acquire a high resolution DEM for every campaign, but we are working on the design of some terrain measurements that allow us a precise evaluation of the errors incurred by using slightly old digital elevation models, such as simultaneous measurements of albedo on different points and comparison with those derived from georeferenced photography.

Unfortunately the instrumentation for this project was a constant battle against the elements. Despite testing the kit under laboratory conditions, the camera case was twice flooded by severe weather conditions, which also prevented collection of data on one occasion. The camera setup was finally destroyed by a lightning strike in March 2007.

GPS survey

Several kinematic and static GPS surveys were conducted to map the extent of the glacier and to georeference tie points for photogrammetric purposes (Figure: 3). Javad's dual-frequency GPS receivers and antennas were used exclusively applying a sampling rate of at least 2 seconds and an elevation cut-off angle of 10 degrees. At all times a nearby reference station mounted on bedrock was occupied to provide geodetic quality measurements for differential positioning at a centimeter level. Thereby, baseline lengths never exceeded a few kilometers. GPS data were postprocessed using Waypoints GrafNav Softwarepackage version 7.70 where precise ephemeris and clock information provided by the International GNSS Service (IGS, final products) were incorporated. In January 2005 the local reference station was linked to the SIRGAS (Sistema de Referencia Geocéntrica para las Américas) which is the regional realization of the International Terrestrial Reference Frame.

Satellite imagery

In order to update the glacier variations at the volcano, several satellite images and aerial photographs were used (Table 1). All the satellite images were geo-located and orthorectified using the regular IGM cartography and available Digital Elevation Models (e. g. SRTM and AIRSAR), (Rivera and others, 2006). Once the satellite images were orthorectified, classification procedures based upon spectral band ratios were applied to account for the glacier extent and snow/ice/debris classification (Paul and others, 2002). Aerial photographs were stereoscopically analyzed and the resulting information was transferred with a Zoom Transfer Scope (ZTS) to the regular cartography, with ice fronts being digitally compared to the satellite (Benson and Follet, 1986). All glacier limits were analyzed using GIS commercial software, such as IDRISI 32 for Windows, Arc-Info version 8.0.1 and PCI Geomatica, allowing an accurate estimation of areas and frontal changes (Figure 2).

Energy balance and melt modelling

We run a modelling experiment to assess the effect of tephra deposition on the glaciated surface of the volcano and its influence on mass balance and runoff. Using meteorological data for twelve days in January, 2007 and the corresponding albedo variations derived from the photographic images, a distributed energy balance model was applied to eastern slopes of the Volcán Villarrica. Thus, we could assess the effect of diminished albedo due to volcanic ash deposition on the mass balance and melt-water production from the volcano glacier. In January 2007 there were no available wind speed data from the AWS. These data were derived from the NOAA archived 1 degree resolution AVN model outputs for the grid cell corresponding to

Volcán Villarrica. The data were chosen at a 750 HPa pressure level, which corresponds to the middle height of the volcano's cone. The model applied (SnowDEM-Snow Distributed Energy balance Model) is explained in detail in Corripio (2003a). It is a distributed, multilayered energy balance model, which takes into consideration radiative fluxes, heat interchange with the atmosphere, evaporation or sublimation and heat flux due to precipitation. Short wave is evaluated according to a detailed parametric radiative transfer model of the atmosphere plus terrain effects (Corripio, 2003b, 2004; Strasser and others, 2004). Longwave is estimated from atmospheric humidity and temperature plus terrain parameters and ground/snow emissivity according to geological characteristics if data are available. Tests on complicated surfaces in the Andes such as penitentes, testify the ability of the model to reproduce snow surface temperature (Corripio and Purves, 2005). Application to a watershed in the Alps for the estimation of meltwater runoff gave values within 6% of measured runoff for a runoff gauge with a 10% accuracy (unpublished data).

RESULTS AND DISCUSSION

The frontal and areal glacier variations of Glaciar Pichillancahue-Turbio have been updated until year 2007 (Table 2). Both main arms of the glacier have continued retreating at similar rates to frontal length changes measured in recent decades (Casassa and others, 2004). These glacier tongues are totally debris covered and only at steep flanks is bare ice visible due to the backwasting ablation process (figure 2). In spite of the insulation provided by the ash and debris covering the ice, the glacier has lost an important area in recent decades, much higher than other debris free glaciers also located on top of active volcanos (Rivera and others, 2006). The present extent of Villarrica's glaciers are shown in figure 2, while recent variations are summarised in table 2.

In order to monitor the glacier at a daily resolution, we used oblique terrestrial photographs that were georeferenced to a DEM with the help of accurate ground control points (GCP) measured on the glacier surface, as shown in Figure 4. This tool can be applied to precisely locate snow features on the surface of the glaciers in areas that are of very difficult access. The eastern upper side of the volcano is constantly swept by ash falls and toxic gases from the crater fumaroles. This made direct surveying impossible without appropriate protective clothes and breathing masks. Thus remote sensing is a more convenient alternative as shown in Figure 5. This figure shows the details of two different images and the changing position of crevasses on the upper section of the volcano. The left image is 25 March 2006 and right image is 14 January 2007. The derivation of flow rates and surface variations using this approach is currently under study and results will be given in a future publication. This preliminary demonstration is shown to illustrate the potential of this technique for high temporal resolution surface monitoring in hazardous or difficult to access environments.

The pattern of tephra dispersion is clearly visible on the georeferenced image of the volcano on 25/12/2005 (Figure 6). The conical shape of the georeferenced image is due to the field of view of the camera. There is a thick tephra layer around the crater rim and a band of darker snow to the SE following the prevailing W and NW winds. The amount and area of tephra deposition depends on the intensity of fumarolic activity and the concurrent winds. It would be possible to model windflow across the volcano, however it is far more difficult to predict the spatial and temporal variability of fumarolic activity. It is therefore very difficult to anticipate the ash dispersion pattern. The only solution is to observe it at relatively high temporal resolution and incorporate the results to any model of the glacier surface.

Here we presents the results for a set of eleven images during a clear sky period from January fifth to January sixteenth, 2007. The albedo of the visible area of the volcano was derived from the photographic images and incorporated into the energy balance model. The albedo derived from the images reveals increasing values toward the fringes of the visible area (the northern and southern slopes). We believe this is a realistic result, as those slopes are away from the prevailing winds and suffer less tephra pollution by volcanic fallout. In fact, a visual inspection of the northern slopes while skiing Villarrica a week earlier showed thick ash layers on the uppermost section of the volcano near the crater and clean, metamorphosed granular snow below that point to an altitude of abut 1800 m a.s.l. Snow was fine grained on the upper section, interspersed with small wind deposits of highly broken precipitation particles (Colbeck and others, 1990), on the lower section it consisted of larger snow grains with high water content.

Previous work suggests that the critical ablation threshold is passed as soon as the tephra forms a continuous layer at the surface, with insulation and melt reduction overriding the influence of albedo lowering (Brock and others, 2007). In this analysis we assumed the critical debris thickness to correspond with an albedo of 11% (based on the broadband albedo of andesitic basaltic tephra, ASTER spectral Library, `http://speclib.jpl.nasa.gov/`), below which snow melt is reduced relative to bare snow surfaces. Spurious high values may be due to errors in the precise boundary between tephra covered and bare snow areas. Theses errors are of the order of two pixels of the original DEM resolution at the borders of the image, or ± 180m. Areas where the viewing angle is very shallow have been masked, but sub-pixel variation in slope may add to this error. Increasing the precision without the use of photogrammetric cameras and a very up to date DEM is unlikely. The resulting ablation map (Figure 7) shows high spatial variability. This variability may be enhanced by post-deposional reworking of the tephra layers, and facilitated by a positive feedback, as surface particles will tend to aggregate while melting on concave surfaces (Drewry, 1972), which are initially caused by differential melt. Of particular note are areas of locally enhanced melting downwind of exposed ash banks in the lower third of the image, and accelerated melting over large areas downwind of the crater, which are exposed to almost continuous airfall tephra deposition. These irregularities are also discernible on any transect along and across the eastern slopes of the volcano, as shown in figure 10. This figure shows the modelled differences in accumulated ablation for a transect along the 2500 m elevation contour and along a transect from the summit crater towards the camera standpoint. Along the elevation isopleth the pattern is approximately symmetrical, with minimum values towards the slopes that are less subject to ash deposition and a maximum on the SE slopes. The horizontal gradient is rather large, with differences in ablation of several cm over a few tens of meters. On the vertical transect, we can observe a clear anomaly, as ablation increases with elevation and reaches a local maximum near the crater (distance 0 to 500 m), where ash depositions are more intense. It then follows an irregular but decreasing trend downslope, as ashes get more dispersed with distance from the source. There are two peaks about 5 km from the crater associated with older ashes that are resurfacing after the overlying snow has disappeared. In these areas tephra is probably thick enough to insulate the underlying ice and reduce melting. Brock et al. (2007) measured a mean daily melt rate of 46 mm w.e. at 3 stakes set on snow with mean albedo 0.51 in the vicinity of the AWS, under similar meteorological conditions in the second half of January 2004. The measured melt rate (12 day cumulative melt = 506 mm) corresponds well with modelled values using photographic derived albedo in January 2007 over large areas of snow with relatively light tephra cover (Figure 7 and Figure 10).

The effects of variable deposition, and redistribution of fallen tephra, on spatial patterns of melt are illustrated by comparison with modelled melt rates when these spatial variations are neglected. Figure 8 shows the differences in modelled cumulative melt rates for the same period, replacing photographic derived albedo with the Brock and others (2000) ageing-curve albedo parameterisation. This parameterisation calculates albedo as a function of accumulated temperatures since the most recent snowfall and assumes albedo decay is caused by snow metamorphism and the build up of impurities over time, but does not account for spatial variation in snow impurity content. While the model with parameterised albedo is able to account for some of the along glacier (vertical) variation in melt rates associated with slower snow metamorphism at higher elevations, cross glacier variation in melt rates, other than that due to aspect and shading is not incorporated and, in particular, the high spatial variability in melt rates immediately below the crater and in the vicinity of exposed ash banks is missed (Figure 8). This demonstrates that using photographic derived albedo provides an improved depiction of the actual spatial variation of surface albedo.

The differences in cumulative ablation between models accounting or not for tephra deposition reach peak values over 40 cm in some spots, however these peak values are probably an overestimation. The errors in this computation are due to a) subpixel slope and albedo variation; b) local areas of very shallow viewing angle where the average DEM slope is steeper and c) projection of cones and mounts into adjacent grids due to almost parallel viewing angle. Therefore only the areas where the viewing angle of camera is over 60 degrees are reliable. This results in differences in ablation of the order of 20 to 30 cm between model runs considering ash cover or clean snow. While at the end of the accumulation season the surface of the glacier is relatively smooth, at the end of the ablation season it presents many concavities a few meters depth and a few tens of meters in diameter (Figure 9). The negative values are areas where the photography derived albedo is higher than the parameterised albedo. This is likely to happen in small concave areas which get more shading from the sun. These small concavities are not registered in the DEM, and therefore a more precise estimation of their albedo would require a higher resolution DEM. The irregular snow surface is likely to be due to a combination of effects by glacier flow and crevasse formation together with differential ablation.

The increase in ablation of snow due to tephra impurities was estimated by Brock and others (2007) to be 8% at the location of the AWS. The same authors recorded rates of melting similar to those produced here for the areas with higher ash depositions. Ablation seems certainly higher further up the slope, as the albedo is lower. This can also be seen from the longitudinal transect (Figure 10). The average modelled increase in ablation for the pixels visible from the camera viewpoint is 13.6% in this study. It is questionable whether this increased ablation and related meltwater production, might have an effect on the glacier dynamics, given the high porosity of the ground. It is, however, likely that it has an impact on the ground water recharge and on runoff further down the valley, with additional implications for the ecological system (e.g. Hauer and others, 1997). A network of piezometers together with runoff gauges would be the ideal instrumentation to detect this effect on water levels, and hopefully will be incorporated in future research programs in the region.

CONCLUSIONS

A number of photographs were obtained from a fixed camera installed at Volcán Villarrica. These photographs have been used to incorporate daily spatial albedo variations into a glacier melt model based on AWS data, SRTM elevation data and GPS measurements on the ground. The modelled ablation shows significantly higher values than previously measured on the volcano (Brock and others, 2007) in areas directly downwind from ash sources, i.e. the crater and exposed tephra banks. These ashes reduce albedo and as a result increase the surface melt rate. The maximum values were found near ash/debris hummocks where winds are blowing material onto the snow. However, large areas of the glacier experience high ablation (low albedo) in the area located downstream to the E and SE from the crater, where airfall tephras are frequently deposited. Another interesting result obtained here, is the posibility of detection of crevassing at the flanks of the volcanic cone. Changing patterns of crevasses could indicate subglacial volcanic activity, as well as glacial ice dynamics. Further research will be needed to extract surface velocities using, e.g. feature tracking in the daily photographs. The frontal variations of the glacier have also been updated, confirming previous receding trends, in spite of the thick insulating debris which mantles most of the glaciers' ablation zones. Continued glacier retreat in spite of the insulating tephra is likely to be due to a combination of reduced accumulation due to decreasing precipitation trends in the region (Bown and Rivera, 2007), rapid melt at exposed ice cliffs along crevasses and possibly enhanced basal melting in areas of high geothermal heating (Rivera et al, 2006).The role of ash deposition on top of the snow surfaces has been discussed here, but more detailed analysis of the mass balance of the glacier needs to be done in order to understand the specific driving factors explaining the retreating trend, especially how the decrease in precipitation observed in the Chilean Lake District (Bown and Rivera, 2007) is affecting the accumulation on the glacier.

ACKNOWLEDGMENTS

This work was sponsored by Fondo Nacional de Ciencia y Tecnología, Chile, (FONDECYT 1040515 and 7050177) and Centro de Estudios Científicos (CECS), Chile. CECS is funded in part by the Millennium Science Initiative and grants from Empresas CMPC. Marcos Rodriguez, Francisca Bown, Andrés Uribe, Gisella Gazitúa, CONAF, SERNAGEOMIN, César Acuña and Robert Koschitzki helped in data collection, preparation of some of the figures, field campaigns and the installation of the equipment. The paper was written while one of the authors (Corripio) was enjoying a grant from the Austrian Science Foundation (FWF project Number M952-N10). We are grateful to the scientific editor Magnus T. Gudmundson and to Lindsey Nicholson and Matt Nolan for their helpful comments.

Table 1. Aerial photographs and satellite images

	OEA*	**LANDSAT MSS****	**SAF***	**SAF***	**GEOTEC***	**ASTER****	**ASTER****	**ASTER****
DD/MM/YY	13/12/1961	08/02/1976	07/01/1983	15/12/1987	30/01/1988	13/02/2003	02/02/2005	24/02/2007
Scale / Resolution (m)	1:50 000	57	1:30,000	1:50,000	1:70,000	15	15	15

* Aerial photographs

** Satellite image

Table 2. Frontal and areal changes of Glaciar Pichillancahue-Turbio

	Period	**Length change** (m)	**Annual length change (m a^{-1})**	area change (km^2)	**Source**
Glaciar Turbio -39°25′, -71°53′	1961-1983	-407	-19	-0.02	Casassa *et al*, 2004
	1983-1987	-43	-9	-0.08	
	1987-1998	-200	-20	-0.35	
	1998-2003	-679	-135	-0.43	
	2003-2005	stable		-0.14	This study
	2005-2007	-60	-30	-0.05	
	1961-2007	**-1389**	**-30**	**-1.07**	
Glaciar Pichillancahue -39°26′, -71°52′	1961-1983	-288	-14	-0.93	Casassa *et al*, 2004
	1983-1987	-51	-11	-0.11	
	1987-1998	-414	-41	-1.05	
	1998-2003	-52	-10	-0.51	
	2003-2005	-136	-68	-0.24	This study
	2005-2007	-95	-48	-0.20	
	1961-2007	**-1036**	**-23**	**-3.03**	

FIGURES

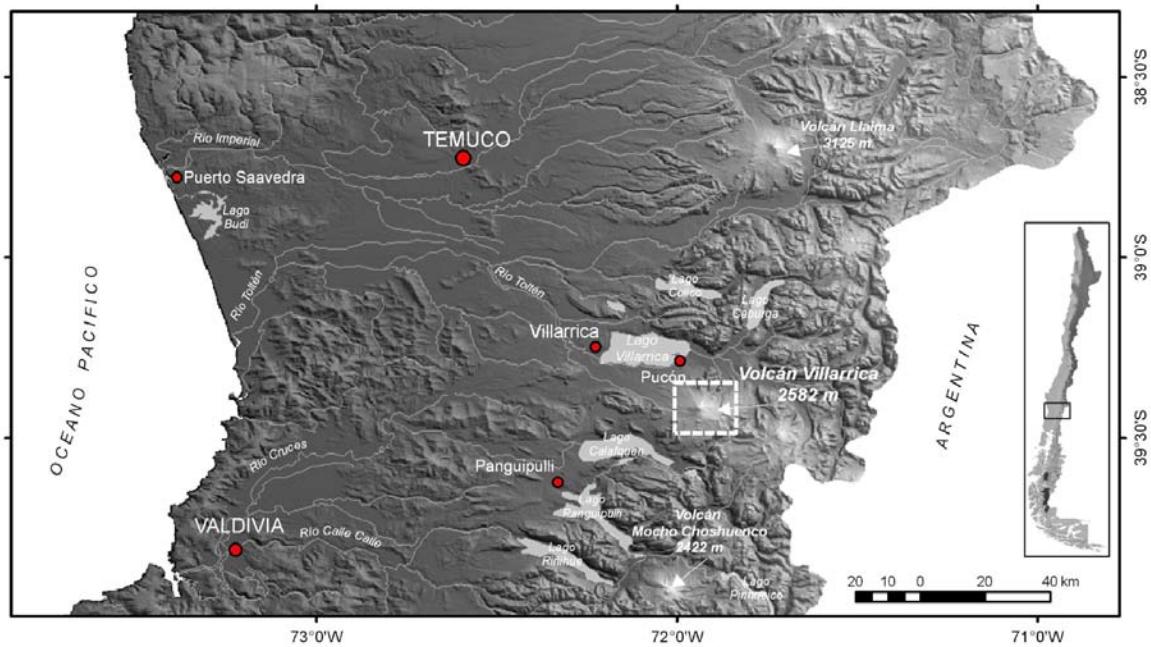

Fig. 1. General location map of Volcán Villarrica

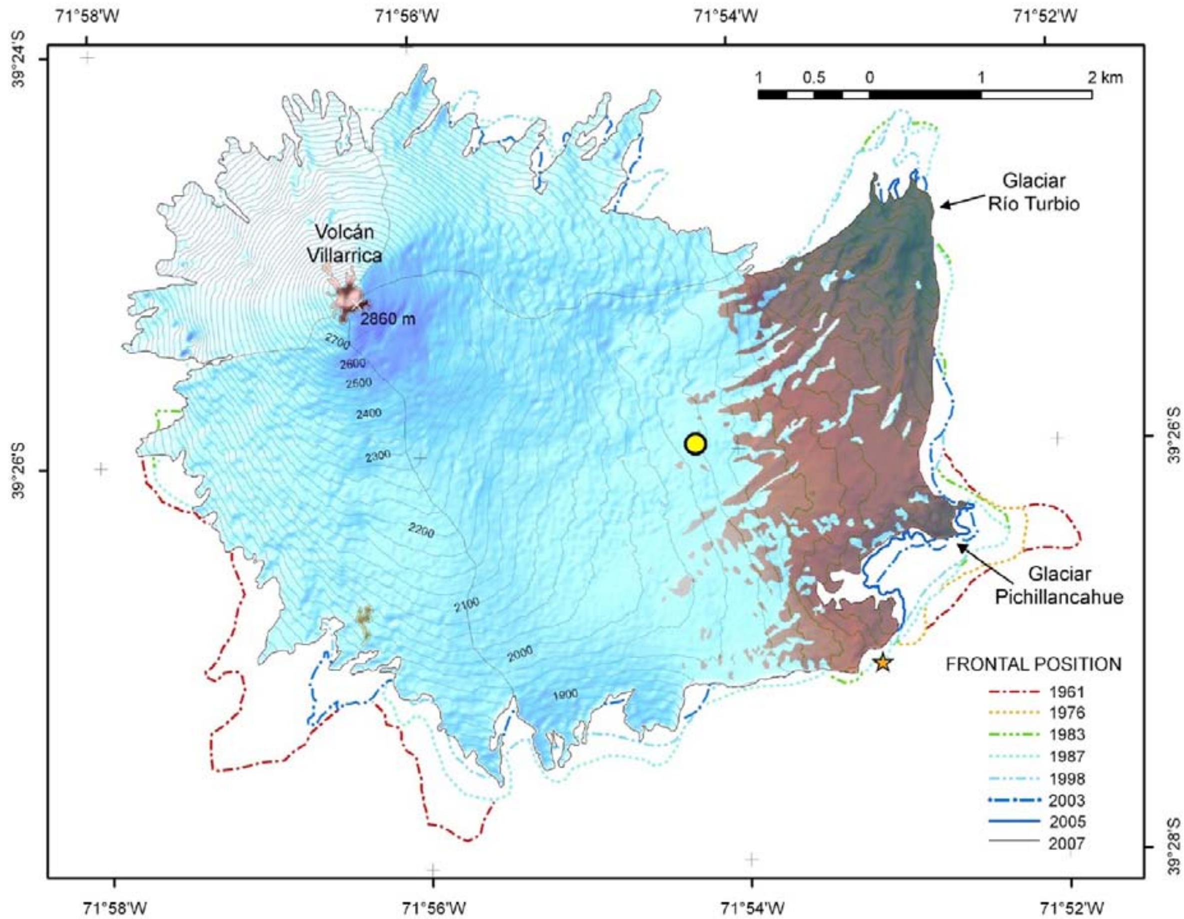

Fig. 2. Glacier variations 1961-2007 at Volcán Villarrica. The yellow dot shows the summer AWS location. The star is showing the location of the Camera, the GPS base Station and the AWS in winter. Blue is snow or ice cover, while brown shows areas of permanently tephra-covered ice.

.

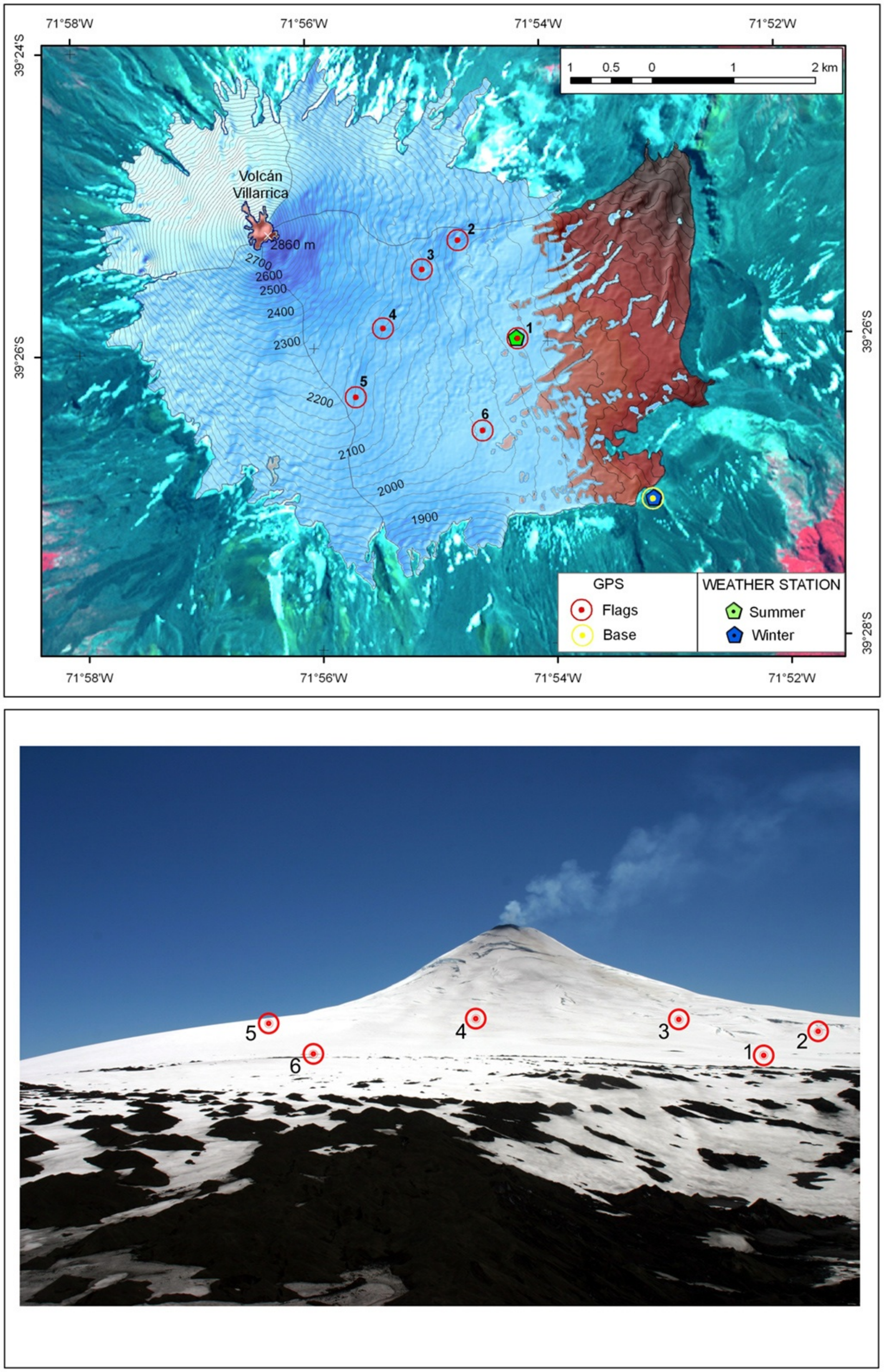

Fig. 3. Location of GPS measurements and the AWS in winter and summer. The lower panel shows the location of the flags installed on the glacier surface which were measured with GPS whilst a photograph was acquired for each site

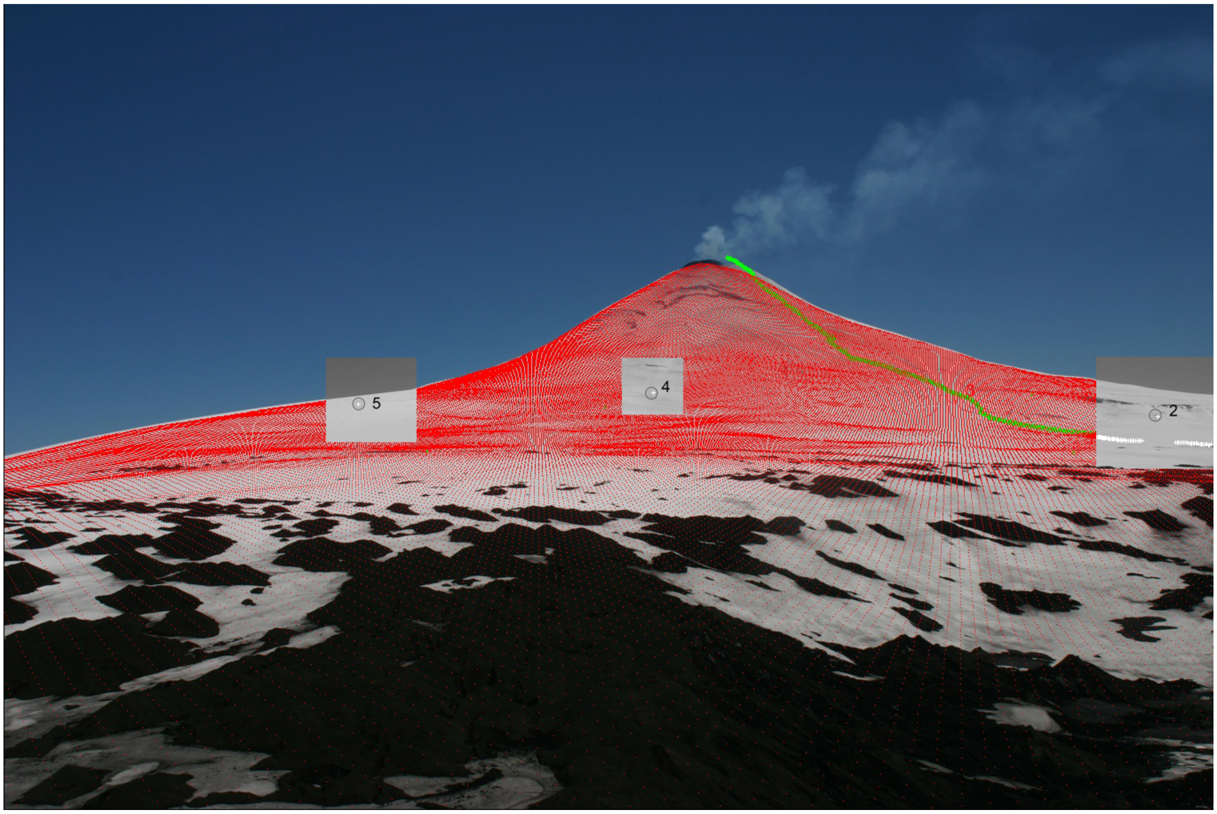

Fig. 4. Image of Volcán Villarrica and superimposed perspective projection of the digital elevation model. Every red dot corresponds to a grid cell in the DEM. Circles in the insets show the location of precise ground control points, which in the terrain where marked by flags visible in the original high resolution photograph

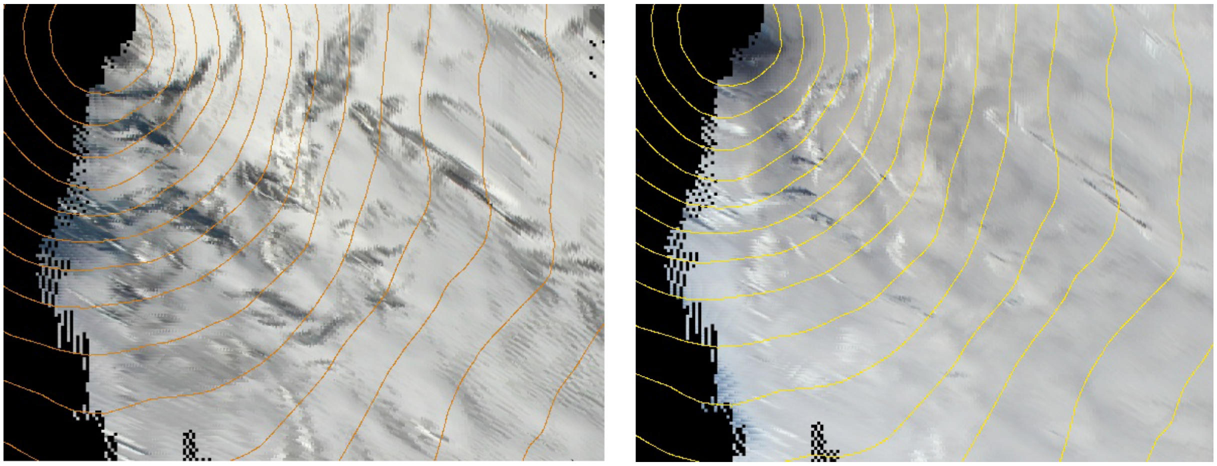

Fig. 5. Detail of two different images showing the changing position of crevasses on the upper section of the volcano. Left image is 25 March, 2006, right image is 14 January, 2007. Black are areas non visible from the standpoint of the camera.

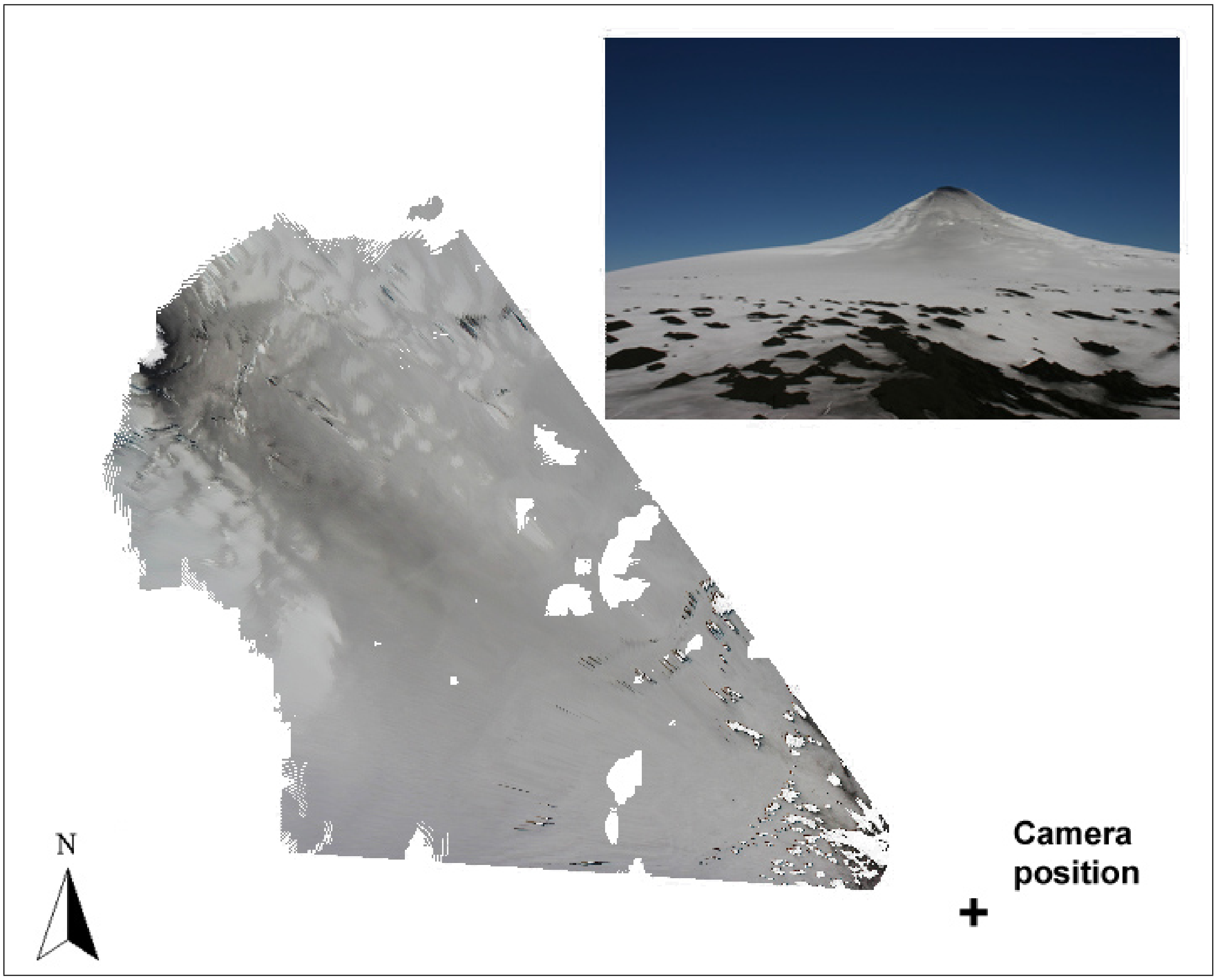

Fig. 6. Pattern of tephra dispersion on the Volcán Villarrica, 25/12/2005. The inset shows the original image. The conical shape of the georeferenced image is due to the field of view of the camera, located on the lower right corner. There is a thick tephra layer around the crater rim and a band of darker snow following the prevailing W and NW winds. White areas in the georeferenced image are not visible from the camera point of view.

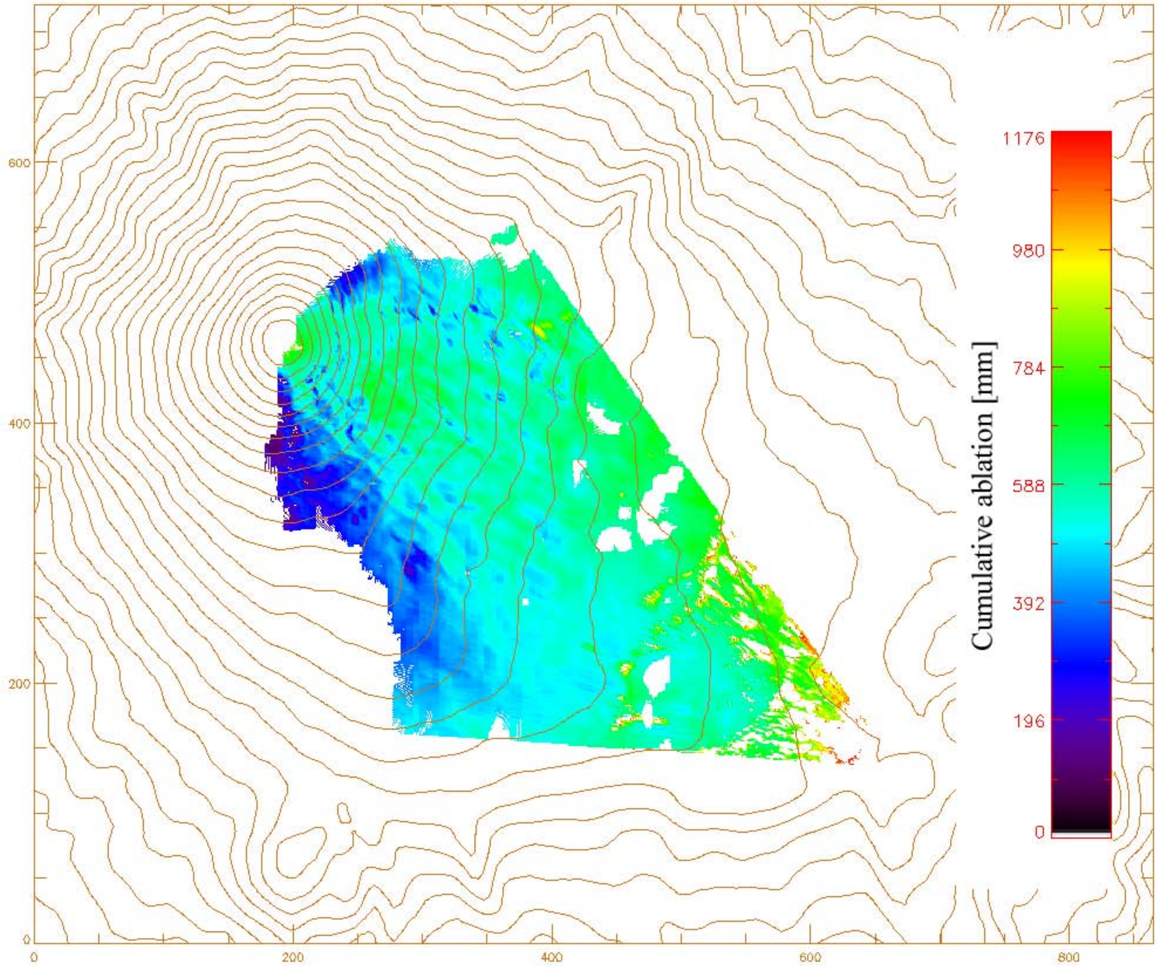

Fig. 7. Map of cumulative ablation from 5 to 16 January, 2007, modelled with albedo derived from daily photographs of the glacier (see Figure 6). The spatial variations are due to the pattern of tephra dispersion, which is more concentrated leeward of the prevailing W and NW winds. Axes units are 10 m.

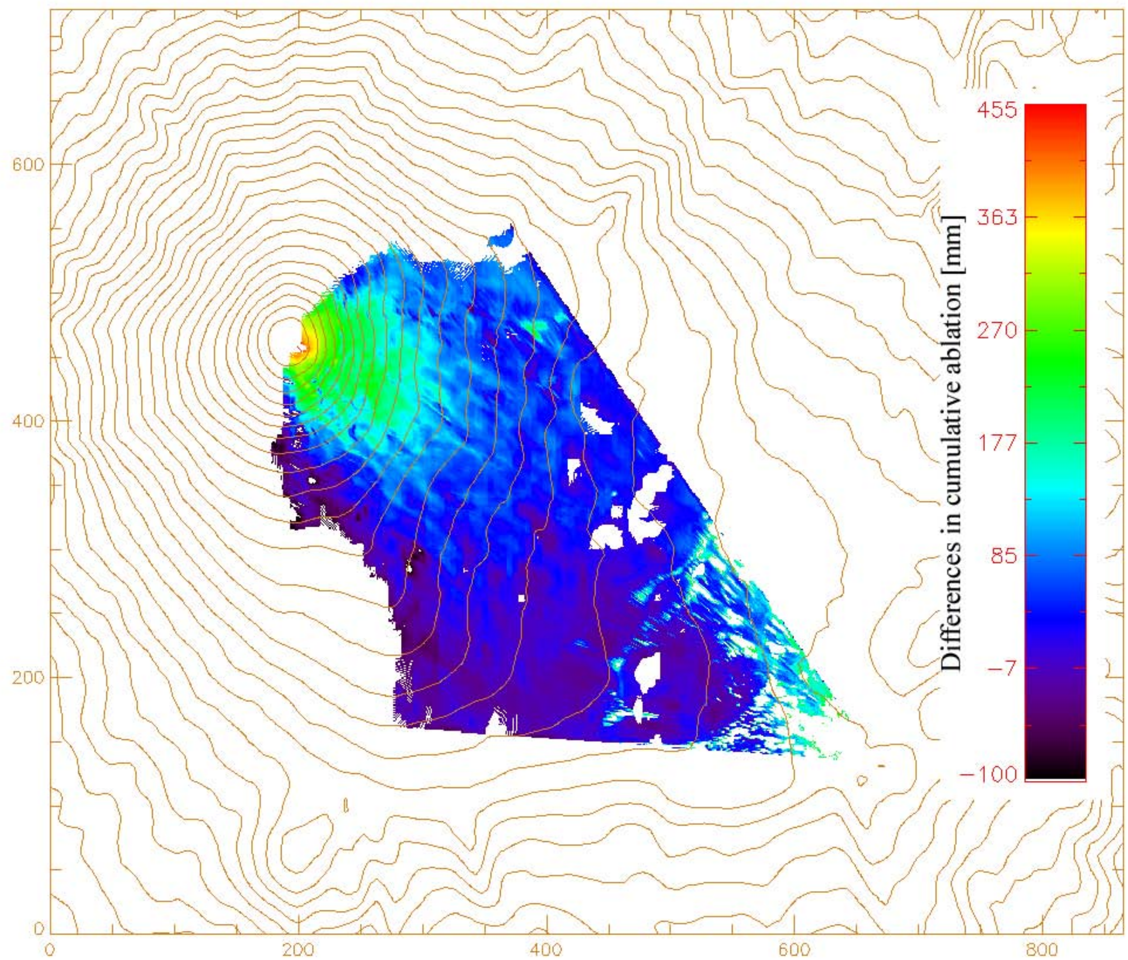

Fig. 8. Map of ablation differences between the observed ash-covered volcano and a hypothetically clean snow surface with albedo parameterised according to Brock and others (2000).

Fig. 9. Photograph of Volcán Villarrica in spring, showing an irregular snow surface, which is likely to be a combination of ice flow and crevassing together with differential ablation.

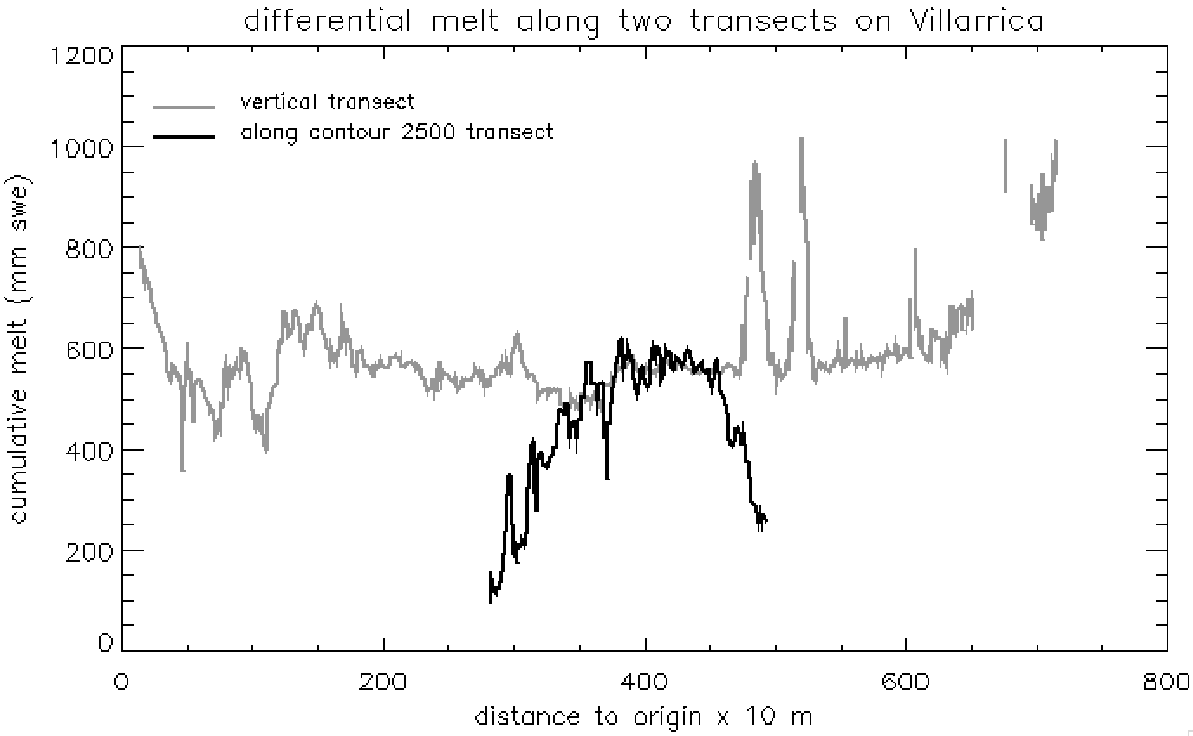

Fig. 10. Profiles of cumulative ablation along the 2500 elevation contour (black) and across a vertical profile from the crater down in direction SE (grey). The origin of the black transect is the NE direction of the 2500 contour, opposite to the viewing direction of the observer. The origin of the vertical transect (grey) is the summit crater.

References

Adhikary, S., Y. Yamaguchi and K. Ogawa, 2002. Estimation of snow ablation under a dust layer covering a wide range of albedo, *Hydrological processes*, **16**, 2853–2865.

Benson, C. and A. Follet, 1986. Application of Photogrammetry to the Study of Volcano-Glacier Interactions on Mount Wrangell, Alaska, *Photogrammetric Engineering and Remote Sensing*, **52**(6), 813–827.

Berk, A, L S Bernstein and D C Robertson, 1989. MODTRAN: A Moderate Resolution Model for LOWTRAN 7, *Tech. Rep. GL–TR–89–012*, Air Force Geophysics Laboratory.

Bown, F. and A. Rivera, 2007. Climate Changes and Glacier Responses During Recent Decades in the Chilean Lake District, *Global and Planetary Change*, doi:10.1016/j.gloplacha.2006.11.015.

Brock, B., A Rivera, G. Casassa, F. Bown and C. Acuña, 2007. The surface energy balance of an active ice-covered volcano: volcan Villarrica, Southern Chile, *Annals of Glaciology*, **45**, 104–114.

Brock, B W, I C Willis and M J Sharp, 2000. Measurements and parameterization of albedo variations at Haut Glacier d'Arolla, Switzerland, *Journal of Glaciology*, **46**(155), 675–688.

Calder, E. S., A. J. L. Harris, P. Peña, E. Pilger, L. P. Flynn, G. Fuentealba and H. Moreno, 2004. Combined thermal and seismic analysis of the Villarrica volcano lava lake, Chile, *Revista Geoló gica de Chile*, **31**(2), 259–272.

Casassa, G., C. Acuña, R. Zamora, E. Schliermann and A. Rivera, 2004. Ice thickness and glacier retreat at Villarrica Volcano, Lara, L.E. and Clavero J., eds., Villarrica Volcano (39.5°S), Southern Andes, Chile, Sernageomin, Santiago de Chile, 53–60, Boletin 61.

Clavero, J. and H. Moreno, 2004. Evolution of Villarrica Volcano, Lara, L. E. and Clavero J., eds., Villarrica Volcano (39.5°S), Southern Andes, Chile, Sernageomin, Santiago de Chile, vol. Boletin 61, 17–27.

Colbeck, S., E. Akitaya, R. Armstrong, H. Gubler, J. Lafeuille, K. Lied, D. McClung and E. Morris, 1990. The International Classification for Seasonal Snow on the Ground, *Tech. rep.*, International Commission of Snow and Ice.

Corripio, J. G., 2003a. Modelling the energy balance of high altitude glacierised basins in the Central Andes, (Ph.D. thesis, University of Edinburgh.

Corripio, J. G., 2003b. Vectorial algebra algorithms for calculating terrain parameters from DEMs and the position of the sun for solar radiation modelling in mountainous terrain, *International Journal of Geographical Information Science*, **17**(1), 1–23.

Corripio, J. G., 2004. Snow surface albedo estimation using terrestrial photography, *International Journal of Remote Sensing*, **25**(24), 5705–5729.

Corripio, J. G. and R. S. Purves, 2005. Surface Energy Balance of High Altitude Glaciers in the Central Andes: the Effect of Snow Penitentes, de Jong, Carmen, Dave Collins and Roberto Ranzi, eds., Climate and Hydrology in Mountain Areas, Wiley, London, chap. 3, 15–27.

Drewry, D J, 1972. Quantitative assesment of dirt-cone dynamics, *Journal of Glaciology*, **18**(63), 431–446.

Fiume, Eugene L, 1989. The mathematical structure of raster graphics, Academic Press, Boston.

Foley, J D, A van Dam, S K Feiner and J F Hughes, 1990. Computer graphics, principles and practice, Adison-Wesley, Reading, Massachusetts.

Fountain, A., R. Jacobel and R. Schlichting, 2005. Fractures as the main pathways of water flow in temperate glaciers, *Nature*, **433**, 618–621.

Fountain, A G and J S Walder, 1998. Water flow through temperate glaciers, *Review of Geophysics*, **36**(3), 299–328.

Fuentealba, G., P. Riffo, H. Moreno and P. Acevedo, 1985. La erupción del volcán Villarrica (octubre, 1984), Ediciones de la Universidad de la Frontera, Temuco, 30 pp.

Fuenzalida, R., 1976. The Hudson Volcano, Gonzales, O., ed., Proceedings of the Symposium on Andean and Antarctic Volcanology Problems, Napoli, Italy, 78–87.

González-Ferrán, 1995. Volcanes de Chile, Instituto Geográfico Militar, Santiago, Chile, 635 pp.

Hauer, F. R., S S. Baron, D. H. Campbell, K. D. Fausch, S. W. Hostetler, G. H. Leavesley, P. R. Leavitt, D. M. Mcknight and J. A. Stanford, 1997. Assessment of Climate Change and freshwater ecosystems of the Rocky Mountains, USA and Canada, *Hydrological Processes*, **11**(8), 903–924.

Kirkbride, M. P. and A. J. Dugmore, 2003. Glaciological response to distal tephra fallout from the 1947 eruption of Hekla, south Iceland, *Journal of Glaciology*, **49**(166), 420–428.

Klohn, E., 1963. The february 1961 eruption of Calbuco volcano, *Bulletin of the Seismological Society of America*, **53**(6), 1435–1436.

Lara, L., 2004. Overview of Villarrica Volcano, Lara, L. E. and Clavero J., eds., Villarrica Volcano (39.5°S), Southern Andes, Chile, Sernageomin, Santiago de Chile, vol. Boletin 61, 5–12.

Metaxian, J., M. Mora S. Araujo and P. Lesaje, 2003. Seismicity related to the glacier of Cotopaxi Volcano, Ecuador, *Geophysical Research letters*, **30**(9), 1483, doi:10.1029/2002GL016773.

Moreno, H., 2000. Mapa de Peligros Volcánicos del volcán Villarrica, *Documento de trabajo 17*, Servicio Nacional de Geología y Minería, escale 1:75000.

Naranjo, J. A. and H. Moreno, 2004. Laharic debris-flows from Villarrica Volcano, Lara, L. E. and Clavero J., eds., Villarrica Volcano (39.5°S), Southern Andes, Chile, Sernageomin, Santiago de Chile, vol. Boletin 61, 28–45.

Paul, F., A. Kääb, M. Maisch, T. Kellenberger and W. Haeberli, 2002. The new remote sensing derived Swiss glacier inventory I: Methods, *Annals of Glaciology*, **34**, 355–362.

Petit-Breuihl, M. and J. Lobato, 1994. Cronología eruptiva histórica del volcán Villarrica, Andes del Sur, Abstracts VIIth Chilean Geological Congress, Concepción.

Rivera, A., F. Bown, R. Mella, J. Wendt, G. Casassa, C. Acuña, E. Rignot, J. Clavero and B. Brock, 2006. Ice volumetric changes on active volcanoes in southern Chile, *Annals of Glaciology*, **43**, 111–122.

Slama, Chester C, Charles Theurer and Soren W Henriksen, eds., 1980. Manual of Photogrammetry, American Society of Photogrammetry, Falls Church, Va, xv, 1056 p.

Stern, C., 2004. Active Andean volcanism: its geologic and tectonic setting, *Revista Geoló gica de Chile*, **31**(2), 161–206.

Strasser, U, J Corripio, F Pellicciotti, P Burlando, B Brock and M Funk, 2004. Spatial and temporal variability of meteorological variables at Haut Glacier d'Arolla (Switzerland) during the ablation season 2001: Measurements and simulations, *Journal of Geophysical Research-Atmospheres*, **109**(D3), D03103.

Witter, J. B. and P. Delmelle, 2004. Acid gas hazards in the crater of Villarrica volcano (Chile), *Revista Geológica de Chile*, **31**(2), 273–277.